PERGAMON

International Journal of Solids and Structures 38 (2001) 3631–3645

INTERNATIONAL JOURNAL OF SOLIDS and STRUCTURES

www.elsevier.com/locate/ijsolstr

# Transient dynamic stress intensity factors around a crack in a nonhomogeneous interfacial layer between two dissimilar elastic half-planes

S. Itou *

*Department of Mechanical Engineering, Kanagawa University, Rokkakubashi, Kanagawa-ku, Yokohama 221-8686, Japan*

Received 10 March 1999; in revised form 30 May 2000

**Abstract**

Dynamic stresses around a crack in a nonhomogeneous interfacial layer between two dissimilar elastic half-planes are obtained. The material constants vary continuously in the layer. An incoming shock stress wave impinges on the crack at right angles to the crack faces. In order to solve the problem, the interfacial layer is divided into several homogeneous layers that have different material properties. The boundary conditions are reduced to dual integral equations using the Fourier–Laplace transform technique. The equations are solved by expanding the differences of the crack faces in a series in the Laplace transform domain. The unknown coefficients in the series are determined using the Schmidt method. The stress intensity factors in the transform domain are inverted numerically in physical space. Using these numerical results, the stress intensity factors for a very thin layer can be estimated. 

*Keywords:* Crack; Dynamic; Fracture; Functionally graded; Composite material

## 1. Introduction

If a diffusion method is used to join a ceramic and a metal, a thin diffusion layer appears between the ceramic and the metal. If an aluminum plate is adhered to a plastic plate through laser beam welding, a thin layer appears, which locks the two materials mechanically. The interfacial zones which join these two materials are relatively weak and are inclined to fracture.

The two-dimensional problem for a cracked interfacial layer between two dissimilar elastic half-planes has been solved by Delale and Erdogan (1988). They assumed that the elastic constants vary continuously across the interfacial layer within the range from the elastic constants of the upper half-plane to those of the lower half-plane and obtained the stress and displacement fields for internal pressure on the crack surfaces.

* Tel.: +81-45-481-5661; fax: +81-45-491-7915.
*E-mail address:* itous001@kanagawa-u.ac.jp (S. Itou).

0020-7683/01/$ - see front matter 
PII: S0020-7683(00)00231-6

The corresponding axisymmetric problem for a cylindrical crack in an interfacial zone between a circular elastic cylinder and an infinite elastic medium for Mode I loading is solved by Itou and Shima (1999).

If composite materials joined by a cracked nonhomogeneous layer are loaded suddenly, it is necessary to clarify the transient dynamic stress intensity factors. Babaei and Lukasiewicz (1998) solved the transient dynamic problem for a crack in a nonhomogeneous layer between two dissimilar elastic half-planes. The crack surfaces are loaded suddenly by anti-plane shear traction, and the dynamic stress intensity factor for Mode III loading is obtained.

In the present paper, dynamic stresses are solved for a crack in a nonhomogeneous interfacial layer between two dissimilar elastic half-planes. On the surfaces of the crack, internal pressure is applied suddenly and the stress intensity factors are obtained for Mode I loading. The material constants in the layer are assumed to vary continuously. In order to circumvent the difficulty associated with the cracked nonhomogeneous layer, the interfacial layer is divided into several homogeneous sub-layers that have different material properties. By letting the number of sub-layers, $m$, approach infinity, the stresses and displacements can be obtained for the nonhomogeneous layer.

Using the Fourier and Laplace transforms, the boundary conditions are reduced to dual integral equations in the Laplace transform domain. In order to solve these equations, the differences of the crack surface displacements are expanded in a series of functions, which are equal to zero outside the crack. In order to satisfy the boundary condition inside the crack, the unknown coefficients in the series are determined using the Schmidt method (Yau, 1967). The stress intensity factors defined in the Laplace transform domain are inverted in physical space using the numerical technique of Miller and Guy (1966). The stress intensity factors are computed numerically for several thicknesses of the layer.

## 2. Fundamental equations

A cracked nonhomogeneous elastic layer ($A$) is denoted by $-H_B \leqslant y \leqslant H_C$ with reference to the rectangular coordinate system $(x, y)$ shown in Fig. 1. A crack is located along the $x$-axis from $-a$ to $a$ at $y = 0$. An upper half-plane ($C$) and a lower half-plane ($B$) are denoted by $H_C \leqslant y$ and $y \leqslant -H_B$, respectively. The shear modulus, Poisson's ratio and the density of the layer ($A$) are represented by $\mu_A$, $v_A$ and $\rho_A$, respectively. Those of the lower half-plane ($B$) and upper half-plane ($C$) are represented using the subscripts $B$ and $C$, respectively. Layer ($A$) is further divided into layer ($A$-1) and ($A$-2). Elastic constants $(\mu_A, v_A, \rho_A)$ most likely vary continuously with respect to $y$ in the interfacial layer, as shown in Fig. 2.

If the displacement components $u$ and $v$ are expressed by two functions $\phi(x, y, t)$ and $\varphi(x, y, t)$ such that

$$u = \partial\phi/\partial x - \partial\varphi/\partial y, \qquad v = \partial\varphi/\partial x + \partial\phi/\partial y, \tag{1}$$

the equations of motion reduce to the following forms:

$$\partial^2\phi/\partial x^2 + \partial^2\phi/\partial y^2 = 1/c_L^2 \times \partial^2\phi/\partial t^2, \qquad \partial^2\varphi/\partial x^2 + \partial^2\varphi/\partial y^2 = 1/c_T^2 \times \partial^2\varphi/\partial t^2, \tag{2}$$

where $t$ is time and the dilatational wave velocity $c_L$ and the shear wave velocity $c_T$ can be given under the plane state of strain as follows:

$$c_L^2 = 2(1-v)\mu/[(1-2v)\rho], \qquad c_T^2 = \mu/\rho. \tag{3}$$

The stresses can be expressed by the equations

$$\begin{aligned}
\tau_{yy} &= -2\mu\partial^2\phi/\partial x^2 + \rho\partial^2\phi/\partial t^2 + 2\mu\partial^2\varphi/\partial x\partial y,\\
\tau_{xx} &= -2\mu\partial^2\phi/\partial y^2 + \rho\partial^2\phi/\partial t^2 - 2\mu\partial^2\varphi/\partial x\partial y,\\
\tau_{xy} &= 2\mu\partial^2\phi/\partial x\partial y + \mu(\partial^2\varphi/\partial x^2 - \partial^2\varphi/\partial y^2).
\end{aligned} \tag{4}$$

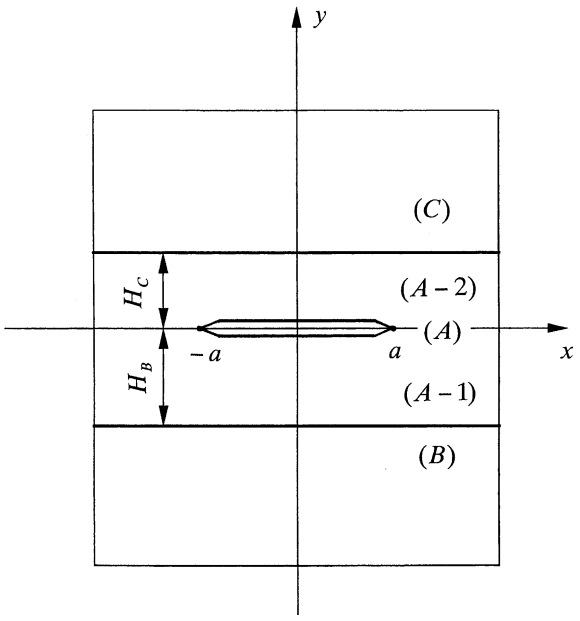


Fig. 1. Geometry and coordinate system.

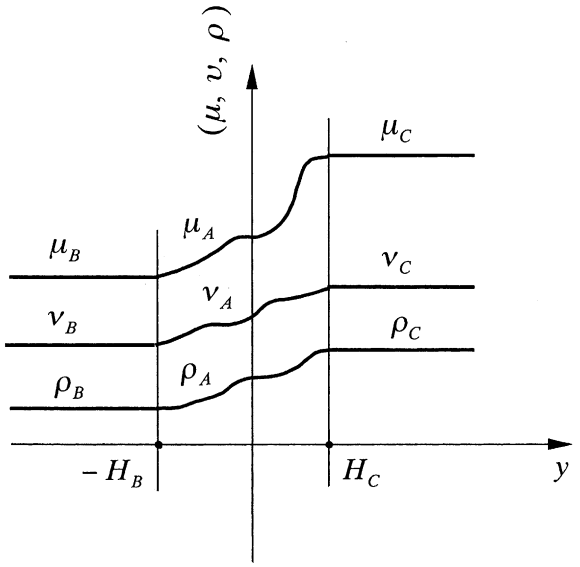


Fig. 2. Shear modulus, Poisson's ratio and density as a function of $y$.

The incident stress wave that propagates along the $y$-axis in the negative direction through the upper half-plane ($C$) can be expressed as

$$\tau_{yyC} = pH(y + c_{LC}t), \tag{5}$$

where $p$ is a constant, $H(t)$ is the Heaviside unit step function and the subscript $C$ indicates variables for the upper half-plane ($C$). If the incident stress wave impinges on the nonhomogeneous interfacial layer, the wave is reflected and refracted in the layer ($A$) in a complicated manner. However, a stress wave similar to that represented by Eq. (5) very likely passes through the nonhomogeneous layer, varying the wave velocity $c_L$ in the layer. Therefore, the boundary conditions for the problem presently being considered can be expressed as follows:

$$\tau_{yyA2} = -pH(t), \quad \tau_{xyA2} = 0 \qquad \text{at } y = 0, \ |x| \leqslant a, \tag{6}$$

$$u_{A2} = u_{A1}, \quad v_{A2} = v_{A1} \qquad \text{at } y = 0, \ a \leqslant |x|, \tag{7}$$

$$\tau_{yyA2} = \tau_{yyA1}, \quad \tau_{xyA2} = \tau_{xyA1} \qquad \text{at } y = 0, \ |x| \leqslant \infty, \tag{8}$$

$$\tau_{yyC} = \tau_{yyA2}, \quad \tau_{xyC} = \tau_{xyA2}, \quad u_C = u_{A2}, \quad v_C = v_{A2} \qquad \text{at } y = H_C, \ |x| \leqslant \infty, \tag{9}$$

$$\tau_{yyA1} = \tau_{yyB}, \quad \tau_{xyA1} = \tau_{xyB}, \quad u_{A1} = u_B, \quad v_{A1} = v_B \qquad \text{at } y = -H_B, \ |x| \leqslant \infty, \tag{10}$$

where subscripts $A1$, $A2$, $B$ and $C$ indicate variables for layers ($A$-1) and ($A$-2) and half-planes ($B$) and ($C$), respectively.

## 3. Division of interfacial layer into sub-layers

The nonhomogeneous interfacial layer ($A$) is divided into several homogeneous sub-layers that have different material properties. The number of the sub-layers, $m$, should be odd rather than even. In order to illustrate the process by which the problem is solved, $m$ is set to three. If $m = 3$, the layer ($A$) is divided into four layers because the sub-layer that contains a crack is divided into two separate layers. More precisely, the interfacial layer ($A$) is divided into sub-layer (1) ($0 \leqslant y \leqslant H_1$), sub-layer (2) ($-H_2 \leqslant y \leqslant 0$), sub-layer (3) ($H_1 \leqslant y \leqslant H_3$) and sub-layer (4) ($-H_4 \leqslant y \leqslant -H_2$), as shown in Fig. 3, where $h_1$, $h_2$, $h_3$ and $h_4$ are the respective thicknesses of the layers. The upper half-plane ($C$) and the lower half-plane ($B$) are numbered by (5) and (6), respectively. For $m = 3$, the shear moduli $\mu_i$ $(i = 1, 2, 3, 4)$ for the four homogeneous layers are as shown in Fig. 4 and are given by the following equations:

$$\begin{aligned} &\mu_4 = \mu_A \quad \text{at } y = -H_4 + h_4/2, \\ &\mu_2 = \mu_A \quad \text{at } y = -H_2 + (h_2 + h_1)/2, \\ &\mu_1 = \mu_2, \\ &\mu_3 = \mu_A \quad \text{at } y = H_1 + h_3/2. \end{aligned} \tag{11}$$

Poisson's ratios $\nu_i$ and densities $\rho_i$ $(i = 1, 2, 3, 4)$ have relationships that are quite similar to those expressed in Eq. (11).

Boundary conditions (6)–(10) can be expressed by the following equations:

$$\tau_{yy1} = -pH(t), \quad \tau_{xy1} = 0 \qquad \text{at } y = 0, \ |x| \leqslant a, \tag{12}$$

$$u_1 = u_2, \quad v_1 = v_2 \qquad \text{at } y = 0, \ a \leqslant |x|, \tag{13}$$

$$\tau_{yy1} = \tau_{yy2}, \quad \tau_{xy1} = \tau_{xy2} \qquad \text{at } y = 0, \ |x| \leqslant \infty, \tag{14}$$

$$\tau_{yy3} = \tau_{yy1}, \quad \tau_{xy3} = \tau_{xy1}, \quad u_3 = u_1, \quad v_3 = v_1 \qquad \text{at } y = H_1, \ |x| \leqslant \infty, \tag{15}$$

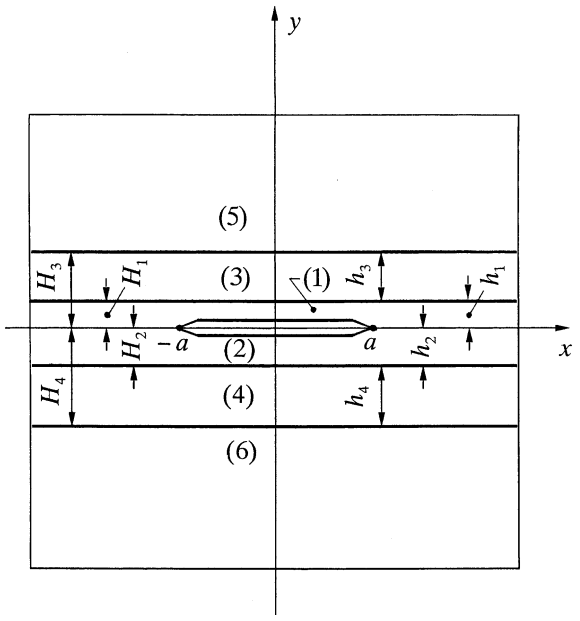


Fig. 3. Interfacial layer replaced by three sub-layers.

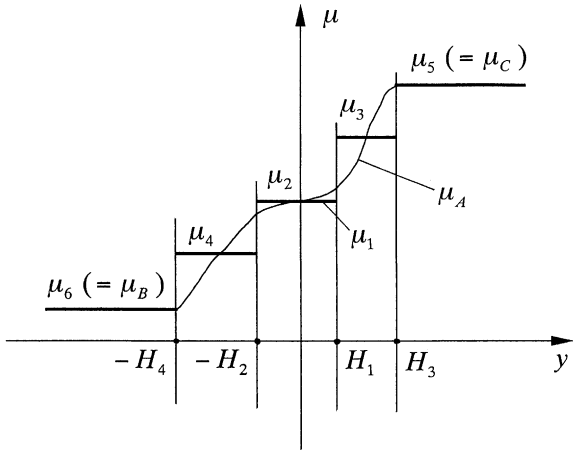


Fig. 4. Shear moduli in the sub-layers used to represent the interfacial layer.

$$\tau_{yy5} = \tau_{yy3}, \quad \tau_{xy5} = \tau_{xy3}, \quad u_5 = u_3, \quad v_5 = v_3 \qquad \text{at } y = H_3, \ |x| \leqslant \infty, \tag{16}$$

$$\tau_{yy2} = \tau_{yy4}, \quad \tau_{xy2} = \tau_{xy4}, \quad u_2 = u_4, \quad v_2 = v_4 \qquad \text{at } y = -H_2, \ |x| \leqslant \infty, \tag{17}$$

$$\tau_{yy4} = \tau_{yy6}, \quad \tau_{xy4} = \tau_{xy6}, \quad u_4 = u_6, \quad v_4 = v_6 \qquad \text{at } y = -H_4, \ |x| \leqslant \infty, \tag{18}$$

where the subscript $i$ indicates the layers $i$ $(i = 1, 2, 3, 4)$ and half-planes $i$ $(i = 5, 6)$.

## 4. Analysis

To find the solution, we introduce the Laplace transforms

$$g^*(s) = \int_0^\infty g(t)\exp(-st)\,\mathrm{d}t, \qquad g(t) = 1/(2\pi i) \times \int_{Br.} g^*(s)\exp(st)\,\mathrm{d}s \tag{19}$$

and the Fourier transforms

$$\bar{f}(\xi) = \int_{-\infty}^{\infty} f(x)\exp(i\xi x)\,\mathrm{d}x, \qquad f(x) = 1/(2\pi i) \times \int_{-\infty}^{\infty} \bar{f}(\xi)\exp(-i\xi x)\,\mathrm{d}\xi. \tag{20}$$

Applying Eqs. (19) and (20) to Eq. (2), we obtain

$$(\mathrm{d}^2/\mathrm{d}y^2 - \xi^2 - s^2/c_{Li}^2)\bar{\phi}_i^* = 0, \qquad (\mathrm{d}^2/\mathrm{d}y^2 - \xi^2 - \varepsilon_i^2 s^2/c_{Li}^2)\bar{\varphi}_i^* = 0, \tag{21}$$

where

$$\varepsilon_i^2 = 2(1-\nu_i)/(1-2\nu_i) \quad (i = 1,2,\ldots,6). \tag{22}$$

The solutions of Eq. (21) are in the following forms for layers $(i)$ $(i = 1,2,3,4)$

$$\bar{\phi}_i^* = A_{1i}\sinh(\gamma_{1i}y) + A_{2i}\cosh(\gamma_{1i}y), \quad \bar{\varphi}_i^* = B_{1i}\sinh(\gamma_{2i}y) + B_{2i}\cosh(\gamma_{2i}y), \tag{23}$$

and for half-planes (5) and (6), the solutions are expressed as

$$\bar{\phi}_5^* = C_5\exp(-\gamma_{15}y), \qquad \bar{\varphi}_5^* = D_5\exp(-\gamma_{25}y), \tag{24}$$

$$\bar{\phi}_6^* = C_6\exp(\gamma_{16}y), \qquad \bar{\varphi}_6^* = D_6\exp(\gamma_{26}y), \tag{25}$$

respectively, where

$$\gamma_{1i} = [\xi^2 + (s/c_{Li})^2]^{1/2}, \quad \gamma_{2i} = [\xi^2 + \varepsilon_i^2(s/c_{Li})^2]^{1/2} \qquad (i = 1,2,\ldots,6) \tag{26}$$

and $A_{11}, A_{21}, B_{11}, \ldots, D_6$ are the unknown coefficients.

Substituting Eqs. (23)–(25) into the Fourier–Laplace transformed expressions of Eqs. (1) and (4), we obtain for layers $(i)$ $(i = 1,2,3,4)$

$$\begin{aligned}
\bar{u}_i^* &= iA_{1i}[-\xi\sinh(\gamma_{1i}y)] + iA_{2i}[-\xi\cosh(\gamma_{1i}y)] + B_{1i}[-\gamma_{2i}\cosh(\gamma_{2i}y)] + B_{2i}[-\gamma_{2i}\sinh(\gamma_{2i}y)],\\
\bar{v}_i^* &= A_{1i}[\gamma_{1i}\cosh(\gamma_{1i}y)] + A_{2i}[\gamma_{1i}\sinh(\gamma_{1i}y)] + iB_{1i}[-\xi\sin(\gamma_{2i}y)] + iB_{2i}[-\xi\cosh(\gamma_{2i}y)],
\end{aligned} \tag{27}$$

$$\begin{aligned}
\bar{\tau}_{yyi}^*/(2\mu_i) &= A_{1i}\{[\xi^2 + \varepsilon_i^2 s^2/(2c_{L1}^2)]\sinh(\gamma_{1i}y)\}\\
&\quad + A_{2i}\{[\xi^2 + \varepsilon_i^2 s^2/(2c_{L1}^2)]\cosh(\gamma_{1i}y)\}\\
&\quad + iB_{1i}[-\xi\gamma_{2i}\cosh(\gamma_{2i}y)] + iB_{2i}[-\xi\gamma_{2i}\sinh(\gamma_{2i}y)],\\
\bar{\tau}_{xyi}^*/(2\mu_i) &= iA_{1i}[-\xi\gamma_{1i}\cosh(\gamma_{1i}y)] + iA_{2i}[-\xi\gamma_{1i}\cosh(\gamma_{1i}y)]\\
&\quad + B_{1i}[-(\xi^2+\gamma_{2i}^2)/2\times\sinh(\gamma_{2i}y)]\\
&\quad + B_{2i}[-(\xi^2+\gamma_{2i}^2)/2\times\cosh(\gamma_{2i}y)].
\end{aligned} \tag{28}$$

For half-planes (5) and (6), the Fourier–Laplace transformed expressions of displacements and stresses are of the form:

$$\begin{aligned}
\bar{u}_5^* &= iC_5[-\xi\exp(-\gamma_{15}y)] + D_5[\gamma_{25}\exp(-\gamma_{25}y)],\\
\bar{v}_5^* &= C_5[-\gamma_{15}\exp(-\gamma_{15}y)] + iD_5[-\xi\exp(-\gamma_{25}y)],
\end{aligned} \tag{29}$$

$$\begin{aligned}\overline{\tau}^{*}_{yy5}/(2\mu_5) &= C_5\{[\xi^2+\varepsilon_5^2 s^2/(2c_{L5}^2)]\exp(-\gamma_{15}y)\}+iD_5[\xi\gamma_{25}\exp(-\gamma_{25}y)],\\ \overline{\tau}^{*}_{xy5}/(2\mu_5) &= iC_5[\xi\gamma_{15}\exp(-\gamma_{15}y)]+D_5[-(\xi^2+\gamma_{25}^2)/2\times\exp(-\gamma_{25}y)],\end{aligned} \tag{30}$$

$$\begin{aligned}\overline{u}^{*}_{6} &= iC_6[-\xi\exp(\gamma_{16}y)]+D_6[-\gamma_{26}\exp(\gamma_{26}y)],\\ \overline{v}^{*}_{6} &= C_6[\gamma_{16}\exp(-\gamma_{16}y)]+iD_6[-\xi\exp(-\gamma_{26}y)],\end{aligned} \tag{31}$$

$$\begin{aligned}\overline{\tau}^{*}_{yy6}/(2\mu_6) &= C_6\{[\xi^2+\varepsilon_6^2 s^2/(2c_{L6}^2)]\exp(\gamma_{16}y)\}+iD_6[-\xi\gamma_{26}\exp(\gamma_{26}y)],\\ \overline{\tau}^{*}_{xy6}/(2\mu_6) &= iC_6[-\xi\gamma_{16}\exp(\gamma_{16}y)]+D_6[-(\xi^2+\gamma_{26}^2)/2\times\exp(-\gamma_{26}y)].\end{aligned} \tag{32}$$

The boundary conditions (14)–(18), which are valid for $|x|\leqslant\infty$, give 18 equations with respect to 20 unknown coefficients. Then, 18 unknown coefficients $iB_{11}$, $iB_{21}$, $A_{12}$, $A_{22}$, $iB_{12}$, $iB_{22}$, $A_{13}$, $A_{23}$, $iB_{13}$, $iB_{22}$, $A_{14}$, $A_{24}$, $iB_{14}$, $iB_{24}$, $C_5$, $iD_5$, $C_6$ and $iD_6$ can be represented by two unknown coefficients $A_{11}$ and $A_{21}$. Namely, all the stresses and displacements can be shown by only two coefficients $A_{11}$ and $A_{21}$. For example, stresses in layer (1) at $y=0$ can be expressed by the equations

$$\begin{aligned}\overline{\tau}^{*0}_{yy1} &= A_{11}k_1^{(1)}(\xi)+A_{21}k_2^{(1)}(\xi),\\ \overline{\tau}^{*0}_{xy1} &= iA_{11}k_3^{(1)}(\xi)+iA_{21}k_4^{(1)}(\xi),\end{aligned} \tag{33}$$

where the expressions of known functions $k_1^{(1)}(\xi)$, $k_2^{(1)}(\xi)$, $k_3^{(1)}(\xi)$ and $k_4^{(1)}(\xi)$ are omitted, and variables having superscript 0 are at $y=0$.

Displacements $\overline{u}^{*0}_1$, $\overline{v}^{*0}_1$, $\overline{u}^{*0}_2$ and $\overline{v}^{*0}_2$ are of the form:

$$\begin{aligned}\overline{u}^{*0}_{1} &= iA_{11}k_5^{(1)}(\xi)+iA_{21}k_6^{(1)}(\xi),\\ \overline{v}^{*0}_{1} &= A_{11}k_7^{(1)}(\xi)+A_{21}k_8^{(1)}(\xi),\end{aligned} \tag{34}$$

$$\begin{aligned}\overline{u}^{*0}_{2} &= iA_{11}k_5^{(2)}(\xi)+iA_{21}k_6^{(2)}(\xi),\\ \overline{v}^{*0}_{2} &= A_{11}k_7^{(2)}(\xi)+A_{21}k_8^{(2)}(\xi),\end{aligned} \tag{35}$$

where the expressions of known functions $k_5^{(1)}(\xi)$, $k_6^{(1)}(\xi)$, …, $k_7^{(2)}(\xi)$ and $k_8^{(2)}(\xi)$ are omitted. From Eq. (34), $A_{11}$ and $A_{21}$ can be solved by $\overline{u}^{*0}_1$ and $\overline{v}^{*0}_1$ as follows:

$$\begin{aligned}A_{11} &= -i\overline{u}^{*0}_1 k_8^{(1)}(\xi)/\Delta-\overline{v}^{*0}_1 k_8^{(1)}(\xi)/\Delta,\\ A_{21} &= i\overline{u}^{*0}_1 k_7^{(1)}(\xi)/\Delta+\overline{v}^{*0}_1 k_5^{(1)}(\xi)/\Delta,\end{aligned} \tag{36}$$

with

$$\Delta = k_5^{(1)}(\xi)k_8^{(1)}(\xi)-k_6^{(1)}(\xi)k_7^{(1)}(\xi). \tag{37}$$

Substituting Eq. (36) into Eq. (33), Eq. (33) reduces to

$$\begin{aligned}\overline{\tau}^{*0}_{yy1} &= -i\overline{u}^{*0}_1 r_1^{(1)}(\xi)+\overline{v}^{*0}_1 r_2^{(1)}(\xi),\\ \overline{\tau}^{*0}_{xy1} &= i(-i\overline{u}^{*0}_1)r_3^{(1)}(\xi)+i\overline{v}^{*0}_1 r_4^{(1)}(\xi),\end{aligned} \tag{38}$$

where the expressions of known functions $r_1^{(1)}(\xi)$, $r_2^{(1)}(\xi)$, $r_3^{(1)}(\xi)$ and $r_4^{(1)}(\xi)$ are omitted. In addition, displacements $\overline{u}^{*0}_2$ and $\overline{v}^{*0}_2$ can be shown by

$$\begin{aligned}\overline{u}^{*0}_{2} &= i(-i\overline{u}^{*0}_1)l_1^{(2)}(\xi)+i\overline{v}^{*0}_1 l_2^{(2)}(\xi),\\ \overline{v}^{*0}_{2} &= -i\overline{u}^{*0}_1 l_3^{(2)}(\xi)+\overline{v}^{*0}_1 l_4^{(2)}(\xi),\end{aligned} \tag{39}$$

where the expressions of known functions $l_1^{(2)}(\xi)$, $l_2^{(2)}(\xi)$, $l_3^{(2)}(\xi)$ and $l_4^{(2)}(\xi)$ are omitted.

In order to satisfy Eq. (13), the differences $(v_1^{*0} - v_2^{*0})$ and $(u_1^{*0} - u_2^{*0})$ are represented in the following series expansions:

$$\begin{aligned} \pi(v_1^{*0} - v_2^{*0}) &= \sum_{n=1}^{\infty} c_n \cos[(2n-1)\sin^{-1}(x/a)] \quad \text{for} |x| \leqslant a, \\ &= 0 \qquad\qquad\qquad\qquad\qquad\quad \text{for} a \leqslant |x|, \end{aligned} \tag{40}$$

$$\begin{aligned} \pi(u_1^{*0} - u_2^{*0}) &= \sum_{n=1}^{\infty} d_n \sin[2n\sin^{-1}(x/a)] \quad \text{for } |x| \leqslant a, \\ &= 0 \qquad\qquad\qquad\qquad\qquad\quad \text{for } a \leqslant |x|, \end{aligned} \tag{41}$$

where $c_n$ and $d_n$ are unknown coefficients. The Fourier transformed expressions of Eqs. (40) and (41) are

$$\begin{aligned} (\overline{v}_1^{*0} - \overline{v}_2^{*0}) &= \sum_{n=1}^{\infty} c_n (2n-1)/\xi \times J_{2n-1}(a\xi), \\ (-i)(\overline{u}_1^{*0} - \overline{u}_2^{*0}) &= \sum_{n=1}^{\infty} d_n (2n)/\xi \times J_{2n}(a\xi), \end{aligned} \tag{42}$$

where $J_n(\xi)$ is the Bessel function. The variables on the left-hand side in Eq. (42) can be modified to the next equation by using Eq. (39). Thus,

$$\begin{aligned} (\overline{v}_1^{*0} - \overline{v}_2^{*0}) &= (-i)\overline{u}_1^{*0}[-l_3^{(2)}(\xi)] + \overline{v}_1^{*0}[1 - l_4^{(2)}(\xi)], \\ (-i)(\overline{u}_1^{*0} - \overline{u}_2^{*0}) &= (-i)\overline{u}_1^{*0}[1 - l_1^{(2)}(\xi)] + \overline{v}_1^{*0}[-l_2^{(2)}(\xi)]. \end{aligned} \tag{43}$$

The variables on the right-hand side in Eq. (42) are identical to those in Eq. (43). Then, $\overline{u}_1^{*0}$ and $\overline{v}_1^{*0}$ can be solved by $c_n$and $d_n$ as follows:

$$\begin{aligned} (-i)\overline{u}_1^{*0} &= \sum_{n=1}^{\infty} c_n (2n-1) l_2^{(2)}(\xi)/(\xi\Delta') \times J_{2n-1}(a\xi) + \sum_{n=1}^{\infty} d_n (2n)[1 - l_4^{(2)}(\xi)]/(\xi\Delta') \times J_{2n}(a\xi), \\ \overline{v}_1^{*0} &= \sum_{n=1}^{\infty} c_n (2n-1)[1 - l_1^{(2)}(\xi)]/(\xi\Delta') \times J_{2n-1}(a\xi) + \sum_{n=1}^{\infty} d_n (2n) l_3^{(2)}(\xi)/(\xi\Delta') \times J_{2n}(a\xi) \end{aligned} \tag{44}$$

with

$$\Delta' = [1 - l_1^{(2)}(\xi)][1 - l_4^{(2)}(\xi)] - l_2^{(2)}(\xi) l_3^{(2)}(\xi). \tag{45}$$

Substituting Eq. (44) into Eq. (36), $A_{11}$ and $A_{21}$ can be represented by the unknown coefficients $c_n$ and $d_n$. Then, stresses that satisfy the boundary conditions (13)–(18) in the Laplace transform domain can be expressed by unknown coefficients $c_n$ and $d_n$. For example, stresses $\tau_{yy1}^{*0}$ and $\tau_{xy1}^{*0}$ are of the form:

$$\begin{aligned} \tau_{yy1}^{*0} &= \sum_{n=1}^{\infty} c_n (2n-1)/\pi \times \int_0^{\infty} Q_1(\xi)/\xi \times J_{2n-1}(\xi a)\cos(\xi x)\mathrm{d}\xi \\ &\quad + \sum_{n=1}^{\infty} d_n (2n)/\pi \times \int_0^{\infty} Q_2(\xi)/\xi \times J_{2n}(\xi a)\cos(\xi x)\mathrm{d}\xi, \\ \tau_{xy1}^{*0} &= \sum_{n=1}^{\infty} c_n (2n-1)/\pi \times \int_0^{\infty} Q_3(\xi)/\xi \times J_{2n-1}(\xi a)\sin(\xi x)\mathrm{d}\xi \\ &\quad + \sum_{n=1}^{\infty} d_n (2n)/\pi \times \int_0^{\infty} Q_4(\xi)/\xi \times J_{2n}(\xi a)\sin(\xi x)\mathrm{d}\xi \end{aligned} \tag{46}$$

with

$$\begin{aligned}
Q_1(\xi) &= \{l_2^{(2)}(\xi)r_1^{(1)}(\xi) + [1 - l_1^{(2)}(\xi)]r_2^{(1)}(\xi)\}/\Delta', \\
Q_2(\xi) &= \{l_3^{(2)}(\xi)r_2^{(1)}(\xi) + [1 - l_4^{(2)}(\xi)]r_1^{(1)}(\xi)\}/\Delta', \\
Q_3(\xi) &= \{l_2^{(2)}(\xi)r_3^{(1)}(\xi) + [1 - l_1^{(2)}(\xi)]r_4^{(1)}(\xi)\}/\Delta', \\
Q_4(\xi) &= \{l_3^{(2)}(\xi)r_4^{(1)}(\xi) + [1 - l_4^{(2)}(\xi)]r_3^{(1)}(\xi)\}/\Delta'.
\end{aligned} \tag{47}$$

Functions $Q_2(\xi)$ and $Q_3(\xi)$ are identical and decrease rapidly as $\xi$ increases. Functions $Q_1(\xi)$ and $Q_4(\xi)$ have the following property when $\xi$ increases,

$$Q_i(\xi)/\xi \to Q_i^L \quad (i = 1, 4), \tag{48}$$

where constants $Q_i^L$ $(i = 1, 4)$ are calculated by

$$Q_i^L = Q_i(\xi_L)/\xi_L, \tag{49}$$

where $\xi_L$ is a large value of $\xi$.

Finally, the remaining boundary condition (12) can be reduced to the equation

$$\begin{aligned}
&\sum_{n=1}^{\infty} c_n G_n(x) + \sum_{n=1}^{\infty} d_n H_n(x) = -p/s, \\
&\sum_{n=1}^{\infty} c_n K_n(x) + \sum_{n=1}^{\infty} d_n L_n(x) = 0 \quad \text{for } |x| \leqslant a,
\end{aligned} \tag{50}$$

where

$$\begin{aligned}
G_n(x) &= (2n-1)/\pi \times \left\{ \int_0^{\infty} [Q_1(\xi)/\xi - Q_1^L] J_{2n-1}(a\xi) \cos(\xi x) \mathrm{d}\xi \right. \\
&\qquad \left. + Q_1^L \cos[(2n-1)\sin^{-1}(x/a)]/(a^2 - x^2)^{1/2} \right\}, \\
H_n(x) &= 2n/\pi \times \int_0^{\infty} Q_2(\xi)/\xi \times J_{2n}(a\xi) \cos(\xi x) \mathrm{d}\xi, \\
K_n(x) &= (2n-1)/\pi \times \int_0^{\infty} Q_3(\xi)/\xi \times J_{2n-1}(a\xi) \sin(\xi x) \mathrm{d}\xi, \\
L_n(x) &= 2n/\pi \times \left\{ \int_0^{\infty} [Q_4(\xi)/\xi - Q_4^L] J_{2n}(a\xi) \sin(\xi x) \mathrm{d}\xi + Q_4^L \sin[2n \sin^{-1}(x/a)]/(a^2 - x^2)^{1/2} \right\}.
\end{aligned} \tag{51}$$

The unknown coefficients $c_n$ and $d_n$ in Eq. (50) can now be solved by applying the Schmidt method (Yau, 1967).

Using the relations

$$\begin{aligned}
\int_0^{\infty} J_n(a\xi)[\cos(\xi x),\ \sin(\xi x)]\,\mathrm{d}\xi = \{&-a^n(x^2 - a^2)^{-1/2}[x + (x^2 - a^2)^{1/2}]^{-n} \sin(n\pi), a^n(x^2 - a^2)^{-1/2} \\
&\times [x + (x^2 - a^2)^{1/2}]^{-n} \cos(n\pi)\} \quad \text{for } a \leqslant x,
\end{aligned} \tag{52}$$

the stress intensity factors in the Laplace transform domain can be expressed as

$$
\begin{aligned}
K_1^* &= \lim_{x\to a+}\sqrt{2\pi(x-a)}\tau_{yy1}^{*0},\\
&= \sum_{n=1}^{\infty} c_n(2n-1)\times(-1)^n Q_1^L/(\pi a)^{1/2},\\
K_2^* &= \lim_{x\to a+}\sqrt{2\pi(x-a)}\tau_{xy1}^{*0},\\
&= \sum_{n=1}^{\infty} d_n\times 2n\times(-1)^n Q_4^L/(\pi a)^{1/2}.
\end{aligned}
\tag{53}
$$

In Sections 3 and 4, stress intensity factors were solved only for $m=3$. However, solutions for $m=1, 5, 7$ can also be obtained in a straightforward manner. The stress intensity factors $K_1^*$ and $K_2^*$ are calculated numerically for $m=1, 3, 5, 7$ and plotted with respect to $1/m$. The stress intensity factors in the cracked nonhomogeneous layer can be obtained only if the layer is replaced by an infinite number of sub-layers. If the numerical results are plotted with respect to $1/m$, the stress intensity factors $K_1^*$ and $K_2^*$ for the interfacial layer, the material constants of which vary continuously with respect to $y$, can be obtained from the values at $(1/m)\to 0$. This process is explained in detail in Section 5.

The inverse Laplace transformations of the stress intensity factors are carried out by the numerical method described by Miller and Guy (1966). When the Laplace transform $g^*(s)$ can be evaluated at discrete points given by

$$s=(\beta+1+k),\quad k=0,1,2,\ldots, \tag{54}$$

we determine coefficients $C_m$ from the following set of equations:

$$\delta\times g^*[(k+\beta+1)\delta]=\sum_{m=0}^{k} C_m k!/[(k+\beta+1)(k+\beta+2)\cdots(k+\beta+1+m)(k-m)!], \tag{55}$$

where $\delta\geqslant 0$ and $\beta\geqslant -1$. If the coefficients are calculated up to $C_{N-1}$, an approximate value of $g(t)$ can be found as

$$g(t)=\sum_{m=0}^{N-1} C_m P_m^{(0,\beta)}[2\exp(\delta t)-1], \tag{56}$$

where $P_m^{(\alpha,\beta)}(z)$ is a Jacobi polynomial. The parameters $\delta$ and $\beta$ must be selected such that $g(t)$ can best be described within a particular range of time $t$.

We have the relation between $g^*(s)$ and $g(t)$ as

$$\lim_{s\to 0}[sg(s)]=\lim_{t\to\infty} g(t). \tag{57}$$

Therefore, the static results of the stress intensity factors in physical space can be obtained using Eq. (57).

## 5. Numerical examples

The transient dynamic stress intensity factors are calculated numerically for ceramic–steel composites and plastic–aluminum composites, the material constants of which are shown in Table 1. In the interfacial layer ($A$), the material constants are assumed to vary linearly with respect to $y$. In addition, the crack is assumed to be situated on the middle surface of the layer. Namely, the $H_C/H_B$ ratio is fixed as 1.0. The nonhomogeneous layer is divided into equal sub-layers. If $m=3$, then $h_3=h_4=(H_B+H_C)/3$, $h_1=h_2=(H_B+H_C)/6$. The accuracy of the numerical calculations are excellent. In order to demonstrate the accuracy of the numerical calculations, calculation process is explained for the worst case: plastic–alumi-

Table 1
Material constants

| Constants | Ceramic | Steel | Plastic | Aluminum |
|---|---|---|---|---|
| $\mu$(GPa) | 119.7 | 79.2 | 0.889 | 26.9 |
| $v$ | 0.27 | 0.3 | 0.35 | 0.34 |
| $\rho(10^3$ kg/m$^3)$ | 3.15 | 7.7 | 1.25 | 2.7 |

Table 2
$Q_i(\xi a)/(\xi a)$ for plastic–aluminum composites[a]

| $(\xi a)$ | $Q_1(\xi a)/(\xi a)$ | $Q_2(\xi a)/(\xi a)$ | $Q_4(\xi a)/(\xi a)$ |
|---|---|---|---|
| 300.01 | −0.1052743 | 0.0029064 | −0.1057867 |
| 300.21 | −0.1052759 | 0.0029018 | −0.1057870 |
| 599.81 | −0.1060325 | 0.0001564 | −0.1060446 |
| 600.01 | −0.1060326 | 0.0001560 | −0.1060446 |

[a] $[H_B/a(=H_C/a)=0.05$, $(sa/c_{L1})=0.2$ and $m=7.]$

Table 3
Values for the left-hand side of Eq. (50) for plastic–aluminum composites[a]

| $x/a$ | $\sum_{n=1}^{12}[c_nG_n(x/a)+d_nH_n(x/a)]/[p/(sa/c_{L1})]$ | $\sum_{n=1}^{12}[c_nK_n(x/a)+d_nL_n(x/a)]/[p/(sa/c_{L1})]$ |
|---|---|---|
| 0.00000 | −0.999847 | 0.000000 |
| 0.04167 | −0.999917 | −0.000026 |
| 0.50000 | −0.999942 | −0.000031 |
| 0.95833 | −1.000009 | 0.000023 |
| 0.99900 | −0.999997 | 0.000007 |

[a] $[H_B/a(=H_C/a)=0.05$, $(sa/c_{L1})=0.2$ and $m=7.]$

num composites for $H_B/a(=H_C/a)=0.05$. First, the values of $Q_i(\xi a)/(\xi a)$ are denoted for $m=7$, $(sa/c_{L1})=0.2$ in Table 2. The table shows that the numerical integrations can be carried out satisfactorily using Filon's method. In Table 3, the values for the left-hand side of Eq. (50) are shown for $m=7$, $(sa/c_{L1})=0.2$. The table shows that the boundary conditions inside the crack are satisfied with good accuracy.

The stress intensity factors $K_1^*$ for the plastic–aluminum composites are calculated for $H_B/a(=H_C/a)=0.05$, $(sa/c_{L1})=0.2$ and are then plotted with respect to $(1/m)$ in Fig. 5. As the number of sub-layers, $m$, approaches infinity, $K_1^*$ rapidly approaches a correct value for a nonhomogeneous interfacial layer. Then, using the values for $(1/m)=1/3$, 1/5 and 1/7 from Fig. 5, we approximate $K_1^*$ using the following equation:

$$K_1^*=a_1(1/m)^3+a_2(1/m)^2+a_3, \tag{58}$$

where constants $a_1$, $a_2$ and $a_3$ can be easily determined. The curve in Fig. 5 is a plot of Eq. (58). It is considered that the value of $\mathrm{d}K_1^*/\mathrm{d}(1/m)$, which is the first-order derivative of $K_1^*$ with respect to $(1/m)$, should be zero as the $m$ approaches infinity. Thereby, $K_1^*$ can be approximated by Eq. (58). The correct value of $K_1^*$ for a cracked nonhomogeneous layer is given by $a_3$ in Eq. (58).

In general, if the value in physical space varies mildly with time, the numerical Laplace inversion can be performed easily as described in a previous paper (Itou, 1983). The present Laplace inversions are just such a case. The stress intensity factors $K_1^*$ and $K_2^*$ are inverted by setting $(\beta=0.0,\delta=0.2,N=13)$ in Eq. (55).

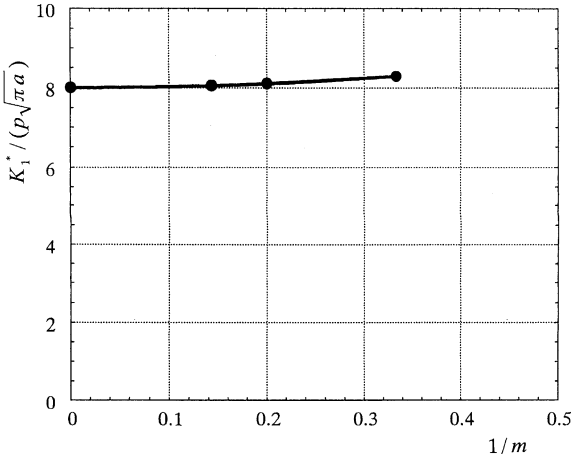


Fig. 5. Curve of $K_1^*$ expressed by $a_1(1/m)^3 + a_2(1/m)^2 + a_3$ for plastic–aluminum composites for $[H_B/a(= H_C/a) = 0.05, (sa/c_{L1}) = 0.2]$.

In Figs. 6 and 7, stress intensity factors $K_1$ and $K_2$ for the ceramic–steel composites are plotted with respect to $c_{L1}t/a$, and Figs. 8 and 9 show these values for the plastic–aluminum composites. The corresponding static values calculated using Eq. (57) are represented by straight lines in these figures.

Here, the method to calculate the static value is explained. The value $K_1/(p\sqrt{\pi a})$ for the plastic–aluminum composites is evaluated for $H_B/a(= H_C/a) = 0.05$. For this case, $K_1^* \times (sa/c_{L1})/(p\sqrt{\pi a})$ are computed numerically for $(sa/c_{L1}) = 0.01$, 0.02, 0.03 and 0.04. Using those four values, $K_1^* \times (sa/c_{L1})/(p\sqrt{\pi a})$ can be approximated by the form:

$$K_1^* \times (sa/c_{L1})/(p\sqrt{\pi a}) = b_1(sa/c_{L1})^3 + b_2(sa/c_{L1})^2 + b_3(sa/c_{L1}) + b_4, \tag{59}$$

where constants $b_1$, $b_2$, $b_3$ and $b_4$ can be easily determined. The curve given by Eq. (59) is drawn in Fig. 10. The static value of the stress intensity factor $K_1/(p\sqrt{\pi a})$ is provided by the value of $b_4$, which is the value of $K_1^* \times (sa/c_{L1})/(p\sqrt{\pi a})$ for $(sa/c_{L1}) = 0$. From the figure, it is clear that the value of $K_1^* \times (sa/c_{L1})/(p\sqrt{\pi a})$

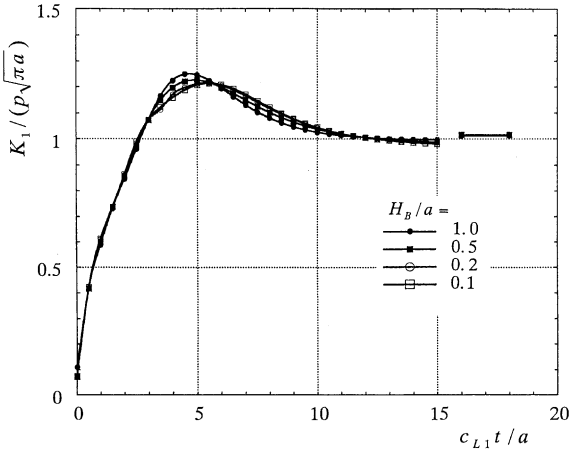


Fig. 6. Stress intensity factor $K_1$ for ceramic–steel composites plotted with respect to $c_{L1}t/a$.

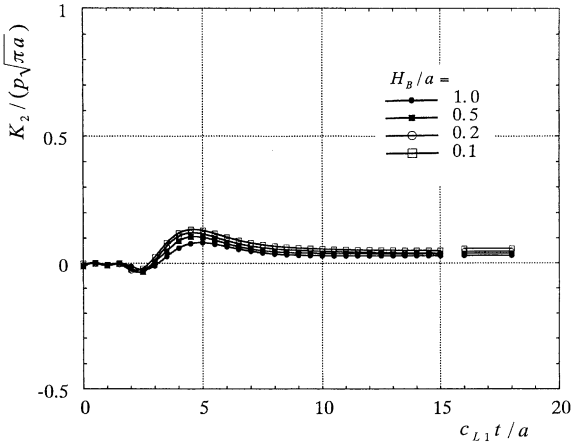


Fig. 7. Stress intensity factor $K_2$ for ceramic–steel composites plotted with respect to $c_{L1}t/a$.

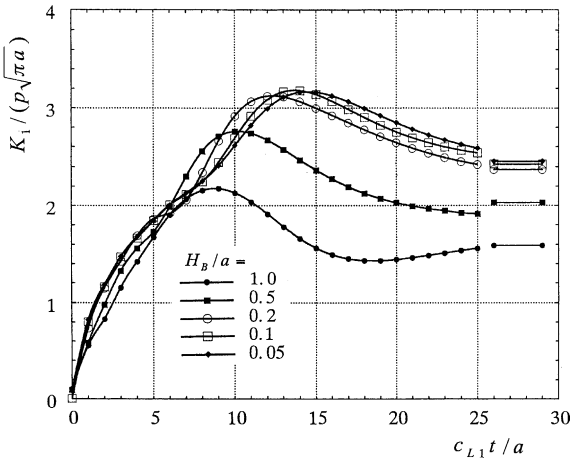


Fig. 8. Stress intensity factor $K_1$ for plastic–aluminum composites plotted with respect to $c_{L1}t/a$.

approaches a fixed value as the value of $(sa/c_{L1})$ approaches zero. Therefore, it is considered that the static values of the stress intensity factors can be calculated precisely.

The peak values of the dynamic stress intensity factors $K_1^{\text{peak}}$ and $K_2^{\text{peak}}$ are divided by the corresponding static values $K_1^{\text{static}}$ and $K_2^{\text{static}}$, respectively, and are denoted in Tables 4 and 5.

## 6. Conclusions

Based on the numerical calculations outlined above, the following conclusions are reached:

(1) For the ceramic–steel composites, the stress intensity factors $K_1$ and $K_2$ are not comparatively affected by the thickness of the interfacial layer. The curves of $K_1$ and $K_2$ for a very thin layer can be approximated by those for $H_B/a = 0.1$.

(2) For the plastic–aluminum composites, the peak values of $K_1$ and $K_2$ are increased as the $H_B/a$ ratio decreases. The curve of $K_1$ for a very thin layer can be approximated by that for $H_B/a = 0.05$. In addition,

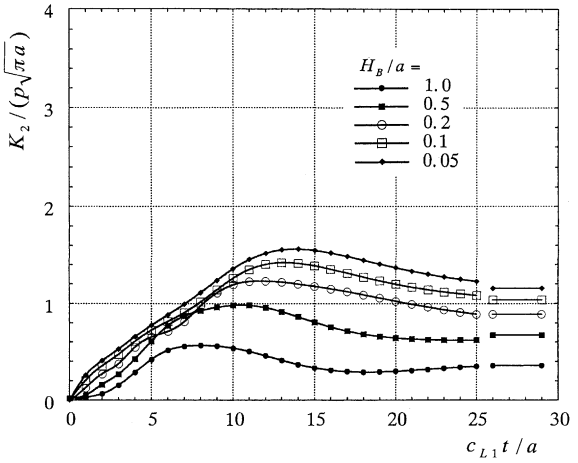


Fig. 9. Stress intensity factor $K_2$ for plastic–aluminum composites plotted with respect to $c_{L1}t/a$.

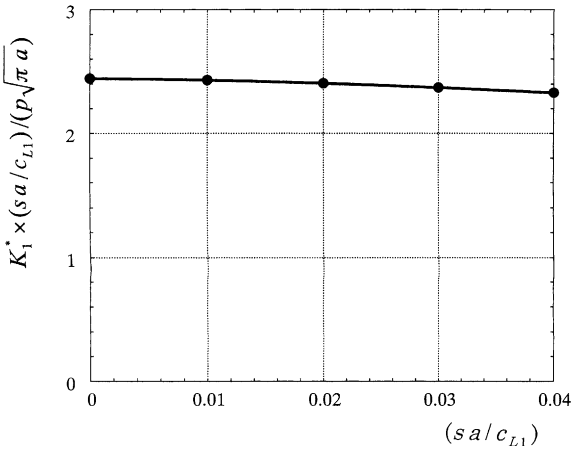


Fig. 10. Curve of $K_1^* \times (sa/c_{L1})/(p\sqrt{\pi a})$ expressed by $b_1(sa/c_{L1})^3 + b_2(sa/c_{L1})^2 + b_3(sa/c_{L1}) + b_4$ for plastic–aluminum composites for $H_B/a(= H_C/a) = 0.05$.

Table 4
$K_1^{\text{peak}}/K_1^{\text{static}}$ ratio for $H_B/a = H_C/a$

| $H_B/a$ | Ceramic–steel composites | Plastic–aluminum composites |
|---|---|---|
| 1.0 | 1.233 | 1.370 |
| 0.5 | 1.207 | 1.360 |
| 0.2 | 1.194 | 1.317 |
| 0.1 | 1.194 | 1.311 |
| 0.05 | | 1.290 |

as the thickness of the interfacial layer approaches zero, $K_2$ falls on a curve that is similar to that for $H_B/a = 0.05$.

Table 5
$K_2^{peak}/K_2^{static}$ ratio for $H_B/a = H_C/a$

| $H_B/a$ | Ceramic–steel composites | Plastic–aluminum composites |
|---|---|---|
| 1.0 | 2.668 | 1.467 |
| 0.5 | 2.658 | 1.460 |
| 0.2 | 2.542 | 1.380 |
| 0.1 | 2.288 | 1.372 |
| 0.05 | | 1.352 |

(3) Both ratios $K_1^{peak}/K_1^{static}$ and $K_2^{peak}/K_2^{static}$ decrease as the $H_B/a$ ratio decreases for both the ceramic–steel composites and the plastic–aluminum composites.

(4) Peak values of $K_1$ for the ceramic–steel composites decrease slightly as the $H_B/a$ ratio decreases. However, for the plastic–aluminum composites, the peak values increase as the $H_B/a$ ratio decreases.

(5) Oscillatory stress singularities appear around an interface crack between two dissimilar elastic materials when the stresses are solved through the Hilbert problem. If two dissimilar elastic half-planes are joined by the interfacial layer, in which the material constants vary continuously, such improper behaviors do not exist unless the thickness is zero and the conventional dynamic stress intensity factors can be defined regardless of the thickness of the interfacial layer.

## References

Babaei, R., Lukasiewicz, S.A., 1998. Dynamic response of a crack in a functionally graded material between two dissimilar half planes under anti-plane shear impact load. Engng. Frac. Mech. 60, 479–487.

Delale, F., Erdogan, F., 1988. On the mechanical modeling of the interfacial region in bonded half-planes. ASME J. Appl. Mech. 55, 317–324.

Itou, S., Shima, Y., 1999. Stress intensity factors around a cylindrical crack in an interfacial zone in composite materials. Int. J. Solids Struct. 36, 697–709.

Itou, S., 1983. Dynamic stress concentration around a circular hole in an infinite elastic strip. ASME J. Appl. Mech. 105, 57–62.

Miller, M., Guy, W.T., 1966. Numerical inversion of the Laplace transform by use of Jacobi polynomials. SIAM J. Numer. Anal. 3, 624–635.

Yau, W.F., 1967. Axisymmetric slipless indentation of an infinite elastic cylinder. SIAM J. Appl. Math. 15, 219–227.